**Biogeosciences
Discussions**

Quantifying wetland methane emissions with process-based models of different complexities

J. Tang[1,2]**, Q. Zhuang**[1,2,3]**, R. D. Shannon**[4]**, and J. R. White**[5]

[1]Dept. of Earth and Atmospheric Sciences, Purdue University, West Lafayette, Indiana, USA
[2]Purdue Climate Change Research Center, West Lafayette, Indiana, USA
[3]Department of Agronomy, Purdue University, West Lafayette, Indiana, USA
[4]Department of Agricultural & Biological Engineering, Pennsylvania State University,
University Park, Pennsylvania, USA
[5]Biogeochemical Laboratories & Center for Research in Environmental Sciences, Indiana
University, Bloomington, Indiana, USA

Correspondence to: J. Tang (tang16@purdue.edu)

Title Page

Abstract | Introduction

Conclusions | References

Tables | Figures

◀ | ▶

◀ | ▶

Back | Close

Full Screen / Esc

Printer-friendly Version

Interactive Discussion

Abstract

Bubbling is an important pathway of methane emissions from wetland ecosystems; however the concentration-based threshold function approach in current biogeochemistry models of methane is not sufficient to represent the complex ebullition process.
5 Here we revise an extant process-based biogeochemistry model, the Terrestrial Ecosystem Model into a multi-substance model (CH_4, O_2, CO_2 and N_2) to simulate methane production, oxidation, and transport (particularly ebullition) with different model complexities. When ebullition is modeled with a concentration-based threshold function and if the inhibition effect of oxygen on methane production and the compe-
10 tition for oxygen between methanotrophy and heterotrophic respiration are retained, the model is a two-substance system. Ignoring the role of oxygen, while still modeling ebullition with a concentration-based threshold function, reduces the model to a one-substance system. These models were tested through a group of sensitivity analyses at two temperate peatland sites in Michigan. We demonstrate that only
15 the four-substance model with a pressure-based ebullition algorithm is able to capture the episodic emissions induced by a sudden decrease in atmospheric pressure. All models captured the retardation effect on methane efflux from an increase in surface standing water which results from the inhibition of diffusion and the increase in rhizospheric oxidation. We conclude that to more accurately account for the effects of
20 atmospheric pressure dynamics and standing water on methane effluxes, the multi-substance model with a pressure-based ebullition algorithm should be used in the future to quantify global wetland CH_4 emissions. Further, to more accurately simulate the pore water gas concentrations and different pathways of methane transport, an exponential root distribution function should be used and the phase-related parameters
25 should be treated as temperature dependent.

1 Introduction

Methane (CH_4) emitted from natural wetlands greatly contribute to its atmospheric budget. Biogeochemistry and atmospheric inversion models estimate the total wetland emissions with a magnitude of 100–230 Tg CH_4 y^{-1}, around 25% of the global emissions into the atmosphere under the current climate condition (Denman et al., 2007). Inverse modeling estimates the strengths of various CH_4 sources and sinks by comparing the model simulated CH_4 concentrations to spatially discrete and temporally continuous observations of the atmospheric CH_4 concentrations. Since all sources/sinks are treated simultaneously in the inversion, the total CH_4 emissions into the atmosphere can be well constrained. However, there are various limitations including the sparse in-situ observation networks of atmospheric CH_4 and unclear sources and sinks due to insufficient understanding of the biogeochemical processes. As a result, the estimates for different sources/sinks from inverse modeling are usually subject to great uncertainties. The process-based models integrate and extrapolate the knowledge from field studies at limited sites to regional and global scales. Because of sparse site-level information and inadequate representation of CH_4 processes in the model, the uncertainties in the quantification from biogeochemical modeling are also substantial (e.g., Walter et al., 2001; Zhuang et al., 2004, 2009; Denman et al., 2007).

To date, a group of process-based models with different complexities have been developed to quantify the spatial and temporal patterns of wetland CH_4 emissions. Among them, the one-substance models are widely used (e.g., Walter and Heimann, 2000; Zhuang et al., 2004; van Huissteden et al., 2006). These models focus on CH_4 only, and assume that methanogenesis and methanotrophy occur in anoxic and oxic zones, respectively, which are spatially separated by the position of water table. In contrast, the two-substance model considers CH_4 and O_2 simultaneously, and the methanogenesis and methanotrophy occur according to the status of both gases in soils (e.g., Arah and Kirk, 2000). This is accomplished by introducing the inhibition effect of O_2 on CH_4 production and the competition for O_2 between heterotrophic

respiration and methanotrophy. As such, CH_4 oxidation and heterotrophic respiration dominate in the oxic zone while CH_4 production dominates in the anoxic zone. The two-substance models have been used in modeling CH_4 emissions from rice paddies (Matthews et al., 2000), and showed reasonable results compared with field measurements. Other existing models are conceptually of either one-substance or two-substance model structure (e.g., Potter, 1997; Zhang et al., 2002).

In biogeochemistry models, three pathways for gas transport are considered: (1) molecular diffusion, (2) plant-aided transport and (3) ebullition, though some models lump the three pathways together (e.g., Cao et al., 1995; Sass et al., 2000; Zhang et al., 2002). Ebullition, if considered explicitly, is often modeled as a threshold phenomenon using the Heaviside function with some universally prescribed threshold concentration of dissolved gas (e.g., Walter and Heimann, 2000; Matthews et al., 2000). Field and analytical studies suggest such a simple algorithm does not fully represent the physical processes of ebullition (Bazhin, 2001, 2004; Baird et al., 2004; Tokida et al., 2005, 2007). Specifically, several factors have not been considered in the concentration-based threshold function algorithms: (1) the composition of the bubbles affected by multiple substances such as CO_2 and N_2; (2) the effects of the hydrostacy affected by water table dynamics and atmospheric pressure variation (Bazhin, 2001; Tokida et al., 2005, 2007) and (3) the ebullition threshold defined in term of gas volumes is fuzzy rather than deterministically predictable because of possible re-dissolution and gas entrapping, during the route of ebullition (Martens and Klump, 1980; Kellner et al., 2006; Coulthard et al., 2009).

In this study, we revise the CH_4 module in a biogeochemistry model, the Terrestrial Ecosystem Model (TEM) (Zhuang et al., 2004) by incorporating the effects of multiple substances in a soil profile and a probabilistic pressure-based algorithm for ebullition. We apply the revised model to two temperate peatland ecosystems to demonstrate the importance of considering the effects of multiple substances in soils on episodic emissions during atmospheric pressure changes (Mattson and Likens, 1990). We also demonstrate the retardation effects of increases in standing water depth on CH_4

effluxes when different model complexities are assumed (Zona et al., 2009).

2 Methods

2.1 Overview

We developed a four-substance CH_4 module within a biogeochemistry model, the Terrestrial Ecosystem Model (Zhuang et al., 2004). The model was calibrated and applied at two temperate peatland sites in Michigan to demonstrate the capabilities of models with different complexities in simulating CH_4 effluxes. A group of sensitivity analyses were conducted to assess the need for a four-substance model with an improved ebullition algorithm.

2.2 The revised CH_4 module

The governing equation for a non-adsorbed substrate in a soil column is:

$$\frac{\partial y}{\partial t} = \frac{\partial}{\partial z}\left(D\frac{\partial y}{\partial z}\right) + P - Q - E - R \qquad \min(0, z_{wt}) \leq z \leq Z \tag{1}$$

where

$$\frac{\partial}{\partial z}\left(D\frac{\partial y}{\partial z}\right) : \text{Diffusion}$$

$$
\begin{aligned}
P : &\quad \text{Production} \\
Q : &\quad \text{Consumption} \\
E : &\quad \text{Ebullition} \\
R : &\quad \text{Plant transport}
\end{aligned}
\tag{2}
$$

and z_{wt} (unit: m) is the water table depth, being negative when it is above the soil surface. For substance i, the bulk concentration y_i (unit: $mol\,m^{-3}$) is related to its aqueous concentration $y_{i,w}$ and gaseous concentration $y_{i,a}$ (unit: $mol\,m^{-3}$) through

$$y_i = \epsilon y_{i,a} + \theta y_{i,w} = (\epsilon + \theta\alpha_i)y_{i,a} \tag{3}$$

where $\epsilon(z,t)$ (unit: m^3 air m^{-3} soil) is air-filled porosity, α_i is the Bunsen coefficient for gas i (see Appendix A for its calculation) and $\theta(z,t)$ (unit: m^3 water m^{-3} soil) is the volumetric soil moisture.

The boundary conditions for Eq. (1) are

$$y_0(t) = y(0,t) \quad \text{for volatiles} \tag{4}$$

$$\frac{\partial y}{\partial z} = 0 \quad \text{for involatiles} \tag{5}$$

at the upper boundary ($z = \min(0, z_{wt})$) and

$$\frac{\partial y}{\partial z} = 0 \tag{6}$$

at the lower boundary ($z=Z$) for all substrates.

2.2.1 Chemistry involved in methane production and consumption

In wetland ecosystems, CH$_4$ is produced primarily through methanogenesis

$$CH_2O + CH_2O \rightarrow CO_2 + CH_4 \tag{7}$$

and consumed through methanotrophy

$$CH_4 + 2O_2 \rightarrow CO_2 + 2H_2O \tag{8}$$

Methanogenesis can proceed in either of the two pathways (Conrad, 1989), i.e. $CO_2 + 4H_2 \rightarrow CH_4 + 2H_2O$, or $CH_3COO^- + H^+ \rightarrow CO_2 + CH_4$, both of which can equivalently be reduced to Eq. (7). Though there are other pathways, e.g. $HCOO^- + \frac{1}{2}H_2O + \frac{1}{4}CO_2 \rightarrow \frac{1}{4}CH_4 + HCO_3^-$, and $CH_3OH \rightarrow \frac{3}{4}CH_4 + \frac{1}{2}H_2O + \frac{1}{4}CO_2$, leading to CH$_4$ production, we assumed they are minor as indicated in previous studies (Conrad, 1989). If one makes the assumption that dissolved oxygen is negligible in the aqueous phase, then the water table serves as a boundary in the soil between the oxic

6126

zone above the water table and the anoxic zone below the water table. Consequently, the equation to solve for the wetland CH_4 profile in a soil column is reduced to a system of a single substance, i.e. CH_4, only. Such was adopted in Walter et al. (2001) and Zhuang et al. (2004), where the bubbling was modeled as a switch-on and -off process

5 with a prescribed threshold CH_4 concentration, $CH_{4,max}$ (unit: $mol\,m^{-3}$).

If one considers the competition for O_2 in CH_4 oxidation and respiration processes, a third stoichiometry is involved:

$$CH_2O + O_2 \rightarrow CO_2 + H_2O \tag{9}$$

With such, we obtained a two-substance model considering both CH_4 and O_2 in a soil

10 profile. Characterization of the aerobic and anaerobic zone in a soil column by the water table in the one-substance system is now revised by introducing the inhibition of O_2 on CH_4 production

$$P_{CH_4} = P_{CH_4}^* \big/ (1 + \eta y_{O_2,w}) \tag{10}$$

where $P_{CH_4}^*$ (unit: $mol\,m^{-3}\,s^{-1}$) is the maximum CH_4 production potential when the

15 environment is completely anoxic, and η (unit: $m^3\,mol^{-1}$) is a parameter representing the sensitivity of methanogenesis to the concentration of dissolved oxygen $y_{O_2,w}$ in pore water. A value of $400\,m^3\,mol^{-1}$ from Arah and Kirk (2000) was used for η. $P_{CH_4}^*$ is defined in Appendix B.

Accordingly, the methanotrophy is restricted by the availability of O_2 as

20 $$Q_{CH_4} = Q_{CH_4}^* \frac{y_{CH_4,w}}{k_{CH_4} + y_{CH_4,w}} \frac{y_{O_2,w}}{k_{O_2} + y_{O_2,w}} \tag{11}$$

where $Q_{CH_4}^*$ (unit: $mol\,m^{-3}\,s^{-1}$) is the oxidation potential when aqueous O_2 and CH_4 are not limited, and k_{CH_4} and k_{O_2} are Michaelis-Menten constants (unit: $mol\,m^{-3}$) for CH_4 and O_2. We use values of $0.44\,mol\,m^{-3}$ water and $0.33\,mol\,m^{-3}$ water, respectively, for k_{CH_4} and k_{O_2} (Arah and Kirk, 2000). $Q_{CH_4}^*$ is defined in Appendix B.

Full Screen / Esc

Printer-friendly Version

Interactive Discussion

The consumption of O_2 due to heterotrophic respiration and CH_4 oxidation is modeled as

$$Q_{O_2} = 2Q_{CH_4} + V_R^* \frac{y_{O_2,w}}{k_R + y_{O_2,w}}$$ (12)

where V_R^* is the maximum rate of respiration when O_2 is not the limiting factor, k_R is the Michaelis-Menten constant, using a value of $0.22\,mol\,m^{-3}$ water (Arah and Kirk, 2000). As in Matthews et al. (2000), we assumed only the process of heterotrophic respiration competes with the process of methanotrophy for O_2, thus V_R^* is twice that of $P_{CH_4}^*$. We also neglected the O_2 consumption by electron acceptor reoxidation (Segers and Leffelaar, 2001; van Bodegom et al., 2001) for the moment. Since no O_2 is produced in the soil, P_{O_2} is set to zero.

Carbon dioxide is produced in methanogenesis, methanotrophy and aerobic respiration:

$$P_{CO_2} = P_{CH_4} + Q_{O_2} - Q_{CH_4}$$ (13)

Just as for O_2 consumption, CO_2 production from electron acceptor reduction (Conrad, 1989) was also neglected here. In the soil, consumption of CO_2 is zero, therefore, $Q_{CO_2} = 0$.

For N_2, we assumed no production and consumption in the soil profile, therefore, $P_{N_2} = Q_{N_2} = 0$.

2.2.2 The pressure-based ebullition algorithm

We revised TEM to consider effects of hydrostacy on ebullition. Tokida et al. (2007) observed an abrupt change in the CH_4 emission rates associated with a decreasing atmospheric pressure, and the mixing ratio of CH_4 in the gas bubbles was no more than 50% (see their Fig. 2). Zona et al. (2009) found that, when the surface standing water increased, the CH_4 efflux was effectively retarded. Such behavior has not been explicitly considered and modeled in the process-based CH_4 models with the conventional

algorithms of ebullition using a prescribed threshold of water dissolved CH_4 (e.g., Walter and Heimann, 2000; Arah and Kirk, 2000; Zhuang et al., 2004). Tokida et al. (2007) suggested a three-substance system, including CH_4, CO_2 and N_2, should be used to model the ebullition. Indeed, Bazhin (2001, 2004) suggested that ebullition is triggered at a certain depth when the total pressure of the water-dissolved gases exceeds the hydrostatic pressure imposed at that depth by the water table and atmospheric pressure. Therefore, the simple concentration-based threshold approach was replaced by an equation of hydrostatic equilibrium. In this study, we considered a four-substance system, i.e. CH_4, O_2, CO_2 and N_2, and ignored other possible trace gases (e.g. argon and hydrogen). We formulated the bubbling criterion as

$$P_s = \sum_i P_{si} = \sum_i \frac{y_{i,\mathrm{w}}(z)}{H_i(z)} \geq P_0 \left(\hat{p} + \frac{b}{z_0} + \frac{z_d}{z_0} \right) = \mathrm{head} \tag{14}$$

where P_{si} is the partial pressure and H_i (see Appendix A for the formula) is the Henry's law constant for gas i, $\hat{p}$ ($=p/P_0$) is the scaled atmospheric pressure, $P_0=10^5$ Pa, $z_0=10$ m, and $z_d=\min(z-z_s, z-z_{\mathrm{wt}})$, and

$$b = \begin{cases} z_s - z_{\mathrm{wt}}, & \text{if } z_{\mathrm{wt}} < 0 \\ \int_{z_s}^{z_{\mathrm{wt}}} \frac{\theta(z)}{\theta_s(z)} dz, & \text{if } z_{\mathrm{wt}} \geq 0 \end{cases} \tag{15}$$

where z_s is the depth of soil surface, set to 0.0; and head (unit: Pa) is the total hydrostatic pressure head imposed by atmosphere and water above depth z. Further we assumed bubbling only occurs below the water table, thus z_d is always non-negative. Note, in Eq. (14), we did not consider the effects of bubble shapes and number of bubbles, which would impact the surface tension between the bubble and water interface and consequently the bubbling criterion (Peck, 1960). We also neglected the change of water distribution caused by the ebullition (Rosenberry et al., 2003), which would cause some bubbles to be trapped and released later.

With Eq. (14), the potential ebullition for gas i at a certain depth z is computed as

$$E_{bi} = \int_{z_{wt}}^{Z} (y_i(s) - \tilde{y}_i(s))\delta(s-z)ds \qquad (16)$$

where the equilibrium bulk concentration is

$$\tilde{y}_i = (\epsilon/\alpha_i + \theta)\tilde{y}_{i,w} \qquad (17)$$

and the equilibrium aqueous concentration is

$$\tilde{y}_{i,w} = \text{head}\frac{P_{si}}{P_s}H_i(z) \qquad (18)$$

and $\delta(s)$ is the Dirac delta function. The potential ebullition computed from Eq. (16) can either be positive or negative, with positive implying bubble formation, and negative implying potential bubble re-dissolution.

To partly account for the fact that a fraction of the bubbles could be re-dissolved during their travel to the atmosphere (e.g., Martens and Klump, 1980), we used the algorithm in Fig. 1 to compute the ebullition. In this probabilistic algorithm, the possibility (p_r) of re-dissolution is proportional to the potential fraction of re-dissolution $\text{abs}(E_b(z))/[\text{abs}(E_b(z))+E(z)]$ (if $E_b(z)$ is negative calculated from Eq. (16)). We modeled the re-dissolution as a yes/no process, if the random number u drawn from a uniform distribution $U[0,1]$ is less than p_r, dissolve the bubbles with an amount of $\text{abs}(E_b(z))$ (or $E(z)$ if $E(z) \leq \text{abs}(E_b(z))$), otherwise, bubbles continue moving upward without re-dissolution, and combine with possible bubbles generated at upper layers.

The algorithm was applied starting from the bottom of soil column to the level of water table. The total ebullition E is either released directly to the atmosphere or added to the soil column, depending on the location of water table. When the water table is at or above the soil surface, the gases carried in the bubbles are directly emitted to the atmosphere; otherwise, they are added to the soil layer right above the water table.

There is an alternative way to implement the above ebullition algorithm, i.e. using the volumetric criteria, such as in Kellner et al. (2006), and most recently in Wania et al.

(2010). Using the ideal gas law, the volume of substances in gaseous phase in equilibrium with the aqueous phase can be computed at all depths. The gas volumes are then compared with some predefined threshold to trigger the bubbles. However, such threshold is fuzzy and varies temporally and spatially due to a group of different factors (Baird et al., 2004; Kellner et al., 2006). Our implementation relates the ebullition directly to the pressure. As such, the ebullition criteria can be determined physically using the available information of gas content and soil water distributions. Also, our algorithm does not need to make any assumption of relative fractions of different gases in the bubbles (Kellner et al., 2006). Arguably, ebullition can even occur without the existence of CH_4, as long as the buoyancy is greater than the weight of the bubble. There are processes have not been accounted for in the algorithm, e.g. entrapped gas due to a wetting process from top of the soil down into the column, which could cause bubble formation (Kellner et al., 2006). Possible ways should be developed in future studies to address such events. It is likely that our algorithm will not always give superior results to that obtained using the volume threshold based method in other studies (e.g., Wania et al., 2010, and comparison is needed). However, its easiness of implementation will make it be readily extended to include more gases in future modeling.

2.2.3 Other transport routes and model implementations

We revised the pathways of diffusion and plant-aided transport in Zhuang et al. (2004) (see Appendix C for details). These and other processes described in previous sections gave the governing equations for CH_4, CO_2, O_2 and N_2 involved in the four-substance model in Appendix C.

As a result, the net CH_4 efflux was computed

$$F_{CH_4} = -\left(D_{CH_4}\frac{\partial y_{CH_4}}{\partial z}\right)_{z=0} + (1-P_{OX})\int_Z^{z_s} R_{CH_4}\,dz$$
$$+\text{Heaviside}\,(z_s - z_{wt})E_{CH_4}(z_{wt}) \tag{19}$$

6131

where P_{OX} takes a value of 0.5 for the one-substance model (Walter and Heimann, 2000) and 0.0, otherwise.

We used the mass balance approach to calculate the diffusive flux to avoid the ambiguity in choosing the depth for computation (Rothfuss and Conrad, 1998). The governing equation Eq. (1) was solved using the method of lines (Schiesser, 1991) with a first order implicit projector-corrector method for the reaction terms. The integration was done with a time step of 2400 s. The soil column was approximated to a depth of 4 m with an exponentially stretching grid (totally 40 nodes) that has finer grid resolution at the top and coarser grid resolution at the bottom (Oleson et al., 2004).

The revised TEM CH_4 module has three different levels of complexity: the one-substance model (S1 model hereafter) was obtained by 1) retaining the processes of methanogenesis and methanotrophy, 2) excluding processes involved with other traces gases and 3) modeling ebullition with the conventional algorithm using a prescribed threshold $CH_{4,max}$ equal to $1.31 \, mol \, m^{-3}$ water (at 25 °C); similarly, the two-substance model (S2 model hence after) was obtained by considering CH_4 and O_2 simultaneously and modeling the ebullition with the concentration-based threshold approach, where $O_{2,max}$ equal to $1.23 \, mol \, m^{-3}$ water (at 25 °C) and $CH_{4,max}$ equal to $1.31 \, mol \, m^{-3}$ water (at 25 °C); when four gases were considered and ebullition was modeled with the new probabilistic pressure-based algorithm, a four-substance model (S4 model hereafter) was obtained.

2.3 Study sites

Two temperate peatlands located in southern Michigan on the Edwin S. George Reserve, a University of Michigan field station were used to test our revised CH_4 module. Three years of measurements from 1991 to 1993 were taken at Buck Hollow Bog and Big Cassandra Bog (42° 27′ N, 84° 1′ W). Buck Hollow Bog is an open peatland covered by a wet lawn of *Sphagnum* species, with a dense cover of *Scheuchzeria palustris*, an arrow-grass. Three flux chambers were grouped in a triangular pattern approximately 10 m apart to measure the net CH_4 flux in the Buck Hollow Bog. Measurements were

taken at four sites at the Big Cassandra Bog. Sites 2 and 3 were used in this study, because these two sites are similar in terms of ecosystem conditions. The sites at the Big Cassandra Bog are dominated by *Sphagnum* and *Polytrichum* mosses and are covered by a dense stand of *Chamaedaphne calyculata*. Measurements of net CH_4

5 fluxes were made using static chambers, and gas samples were collected and analyzed within 3–4 days of collection on a Shimadzu GC-14A gas chromatograph with a flame ionization detector. Environmental variables including water table depth and soil temperature from 5 cm above the peat surface into 100 cm in the peat column were monitored and used as driving data for the model in this study. Available pore water

10 concentration profiles (with a detection limit 0.1 µM) were also used in our assessment of the model. For a detailed description of the study sites and assessment of measurements, readers can refer to Shannon and White (1994).

2.4 Standard simulations

Standard simulations were conducted for each site with parameters calibrated by trial

15 and error to get the simulated fluxes and pore water concentrations as close as possible to the measurements (Table 1), so that the differences between different model simulations were mainly due to different model formulations. We used the measured water table depth and soil temperature as environmental forcing. Since no site-specific measurements of atmospheric pressure were available, we simply set total pressure

20 to 1 atm, a standard number that has been used in other model studies (Walter and Heimann, 2000; Zhuang et al., 2004). For soil porosity, we assumed a value of 0.83 v v^{-1} for depths shallower than 0.5 m, linearly decreasing to 0.53 v v^{-1} at 0.9 m, and constant at 0.53 v v^{-1} to the lower boundary of 4 m. The scaled NPP data (Fig. 2) required to model CH_4 production were derived from simulations using TEM driven

25 with monthly climate data (Mitchell et al., 2004). For the atmospheric mixing ratio of the gases involved, we assume 0.209 v v^{-1} for O_2, 0.781 v v^{-1} for N_2, 385 ppmv for CO_2 and 1740 ppbv for CH_4 (Forster et al., 2007).

2.5 Model sensitivity studies

To test the responses of the different models to water table dynamics, we ran our models with the time series of water table depth artificially increased or decreased over a specific time period during the emission season. As shown in Fig. 3, for the Buck Hollow site, we increased the water table by 10 cm between ordinal day 150 and 160 (1 January 1991 was set to ordinal day 1), and decreased by 10 cm between ordinal day 590 and 600; for the Big Cassandra site, we increased the water table depth by 10 cm between ordinal day 135 and 145, and decreased by 10 cm between ordinal day 689 and 699. These days were chosen such that the differences were significant enough to be identified. The results were analyzed by comparing simulations with those from standard simulations.

Two sets of experiments were used to test the model response to atmospheric pressure change. First, we conducted sensitivity simulations using a time series of artificially perturbed low pressure or high pressure events (specifically 930 hPa low and 1045 hPa high) on two arbitrarily chosen days during the high-emission season in summer (Fig. 4). The effect of changing atmospheric pressure was analyzed by comparing the change in pathways of CH_4 transport with that from the standard simulation. This was used to analyze whether the response is physically consistent or not. A second test was carried out to test the overall effect of atmospheric pressure variability using a time series of atmospheric pressure (Fig. 5) extracted from the European Centre for Medium-Range Weather Forecasts (ECMWF) Interim re-analysis dataset at the grid that encompass the site for the same time period of measurement. The response was again analyzed by comparing the results to the standard simulations.

3   Results and discussion

3.1   Comparisons between standard model simulations and site-level nobservations

All models resulted in similar CH_4 fluxes (Table 2). Specifically, for the Buck Hollow site, the S1, S2 and S4 models all captured the temporal variability of the CH_4 fluxes (Fig. 6). Because of the probabilistic feature of S4 model, mulitple runs were conducted. The differences from these multiple runs were indistinguishable because the emission routes at these two sites were dominated by plant-aided transport, and bubble redissolution rarely occured. The mean from an ensemble simulation of size four was shown for comparison. The S4 model performed best in terms of linear fitting and the root mean square error (RMSE) against the measurements (Table 2). The S1 model presented the second best results, with the simplest model structure. In the S1 simulation, the maximum production rate was at least an order of magnitude smaller than those of S2 and S4 models because it included no inhibition effect of O_2 on methanogenesis (Table 1). The maximum oxidation rates ($\hat{O}_{CH_4}$) were similar in magnitude. Note that the simulations (except S4) were not very sensitive to $\hat{O}_{CH_4}$.

The importance of different CH_4 transport pathways varied in different models (Fig. 6). Diffusion played a significant role in the release of CH_4 into the atmosphere, even though plant transport remained the dominant pathway in S4 simulations. In S2 simulations, plant transport accounted for more than 90% of the efflux into the atmosphere. The modeled diffusion contribution to efflux reached a short-term maximum between day 170 and 180 in the S1 simulations. This was due to a sudden and substantial decrease in water table from above the peat surface to below the peat surface (Fig. 3). This increased the concentration gradient of the CH_4 near the peat surface and thus increased diffusion. Such short-term changes were also found in the S2 and S4 simulations, but with smaller magnitudes. All the models suggested the efflux through ebullition was small, which agrees with measurements (Shannon and White, 1994). In

S4 simulation, the ebullition played a bigger role than that did in S1 and S2 simulations.

S1 performed the best in simulating pore water concentrations; followed by the S2 model and then the S4 model (Fig. 6). For 12 June 1993, none of the models presented a satisfying result. The discrepancy might be due to the nonlinearities of the transient simulations. For example, the pore water concentrations at a certain day were impacted by results in previous days. Uncertainty in the driving data (e.g. soil temperature) is another source of such discrepancy.

At the Big Cassandra site, the simulated effluxes were less satisfying than the Buck Hollow Bog site, though S4 model performed the best, followed by the S2 model and then S1 model. Particularly for the second half year of 1991 and the year 1992, the results compared poorly with measurements. This underperformance may be due to an inadequate representation of the methanogenesis substrate, which was simulated in TEM but has not been specifically calibrated for wetland ecosystems. At this site, plant transport was the most important pathway, and ebullition was relatively unimportant. All three models presented similar results for pore water concentrations (Fig. 6).

3.2 Model sensitivity analyses

3.2.1 Sensitivity to water table change

We found that the response to a 10 cm change in surface standing water caused a change in the CH_4 efflux by as much as $-50\sim300$ mg CH_4 m^{-2} d^{-1} (Fig. 7). Such responses depend on the site characteristics and the model complexity. At the Big Cassandra site, S1 and S2 model gave stronger response in effluxes to the water table increase than S4 model did, while the opposite occurred for the water table decrease. At the Buck Hollow site, the responses of different models to the water table change were sort of similar, but S1 gave a much stronger response to the water table decrease than S2 and S4 did. Nevertheless, all the models successfully predicted the retardation effect of an increase in surface standing water on CH_4 efflux (Fig. 8). This can be explained by the low diffusivity of gases in water relative to air. A higher column of

surface standing water represents a longer distance of diffusion before gas can escape into the atmosphere. This phenomenon may account for CH_4 accumulation in the peat column, which in turn enhances plant mediated transport, as well as the oxidation of CH_4 in the rhizosphere, thus decreases the efflux. When water table depth decreases,
5 the diffusion distance is reduced, and efflux to the atmosphere increases (Fig. 8). In places where emergent vascular plants are sparse, a decrease in water table depth could enhance CH_4 efflux through ebullition. This was tested by removing the plants in our simulations. Field data from Buck Hollow site demonstrate this phenomenon (Shannon et al., 1996) and this behavior was confirmed in the S4 simulations as S4
10 is the only model that considers the effect of hydrostatic pressure change (result not shown).

3.2.2 Sensitivity to atmospheric pressure change

For the first sensitivity test of the models to atmospheric pressure change, S1 and S2 models showed much weaker ($10^1 \sim 10^2$ weaker) responses than that of the S4
15 model (Fig. 9). In both S1 and S2 models, a change in atmospheric pressure can only affect the atmospheric concentration of the gases. Given the small feasible range of atmospheric temperature change and atmospheric pressure change, the change in atmospheric CH_4 concentration is small, implying a small change of the diffusion rate and thus the methane efflux in these two models. However, in the S4 model, the
20 atmospheric pressure was further related to the ebullition fluxes. When a low atmospheric pressure occurred, the ebullition criterion became less restrictive, and bubbles were more easily formed, enhancing the ebullition. In this simulation, a decrease in atmospheric pressure could trigger an episodic increase in CH_4 efflux by as much as $120\,\mathrm{mg\,CH_4\,m^{-2}\,d^{-1}}$ at the Buck Hollow site and as much as $80\,\mathrm{mg\,CH_4\,m^{-2}\,d^{-1}}$ at
25 the Big Cassandra site, comparable to the enhancement due to a decrease in surface standing water table depth.

When the results from the sensitivity test to transient atmospheric pressure were analyzed, we found very different fluxes simulated by the different models (see Fig. 10).

For instance, in cases of low atmospheric pressure events at the Buck Hollow site, the S4 model usually predicts higher fluxes through enhancement of ebullition. The S1 model responded to the atmospheric pressure change with a negligible magnitude. The S2 model also responded significantly to the change of atmospheric pressure,
5   but showed lower fluxes in accordance with a lower concentration of atmospheric CH_4 at the upper boundary. In cases of high pressure events, S4 reduced the fluxes by suppressing the ebullition, and S2 enhanced the fluxes due to a higher atmospheric concentration of CH_4 at the upper boundary, and S1 responded to such change with negligible magnitudes. Similar results were found at the Big Cassandra site. The
10 change of atmospheric pressure also changed the rate of plant aided transport and diffusion, however, in our formulation of the algorithm, the ebullition is the preferred route if it is triggered (which we also believe is true in the field). When the cumulative differences were analyzed, we found for a three year period at the Buck Hollow site, the S4 predicted around $2000\,\mathrm{mg\,CH_4\,m^{-2}\,y^{-1}}$ using the transient atmospheric pres-
15 sure data than using the standard 1 atm pressure. The S2 model, however, predicted $2000\,\mathrm{mg\,CH_4\,m^{-2}\,y^{-1}}$ lower when the transient atmospheric pressure was used. Similar results were found at the Big Cassandra site, with smaller magnitudes of differences, in accordance with the lower emission rate.

3.3 The importance of using temperature dependent parameters

20 In our standard and sensitivity simulations with the revised CH_4 module, we treated the phase-related parameters, such as diffusivities, Henry's law constants and Bunsen coefficients as temperature dependent. Analysis showed that, within the typical temperature range (e.g., −5 to 30 °C), the diffusivity of CO_2 in water changed ± 5%, the Henry's law constant and Bunsen coefficient changed ± 50% (results not shown). For
25 CH_4, its diffusivity in air changed ± 10% and in water changed ± 5%, but the Henry's law constant and Bunsen coefficient changed ± 40%. To test if fixing these parameters at a specific reference temperature could significantly affect the results, we conducted a set of simulations with the phase-related parameter values corresponding to

a reference temperature of 12.5 °C.

We found, for the S1 model, that the temperature dependence of these parameters did not change the efflux significantly (Fig. 11). However, compared to the standard simulation, both the S2 model and S4 models predicted a higher CH_4 efflux during high emission periods. Given that soil temperatures at the two sites were often above the reference temperature during the high-emission summer season, the lower solubility computed with reference temperature allowed less O_2 and CH_4 to be stored in the soil, given almost the same rate of CH_4 production. Further, considering the inhibition effect of O_2 on methanogenesis and the stimulus effect of O_2 on methanotrophy, the higher emissions associated with the S2 and S4 models using coefficient values at the reference temperature is then explained as a stimulus of gas transport to the atmosphere. We concluded that fixing phase-related parameters at their reference temperature values is safe for the S1 model, but that temperature-dependent parameters should be used in the S2 and S4 models.

3.4 The role of root density distribution

Previous CH_4 modeling has used a linear function for the vertical distribution of root density (e.g., Walter and Heimann, 2000; Zhuang et al., 2004; also see Eq. (D-2) in Appendix D). However, root biomass is often found to be exponentially distributed (Jackson et al., 1996), and an exponential root distribution could also be used (e.g., van Huissteden et al., 2006). Here we implemented both linear and exponential root distribution functions in our revised CH_4 module to test if they make a difference on CH_4 effluxes (Tables 1–4) and pore water concentrations.

We found the contributions from different pathways were different when two different root density distribution functions were used (Figs. 6 and 12). In the standard simulation using an exponential root density distribution function, ebullition played a minor role, whereas in the simulation employing a linear root density distribution, the ebullition was more significant, particularly in the S2 and S4 models. The ebullition was enhanced more at the Big Cassandra site than at the Buck Hollow site, suggesting the

responses of the models to two different root distribution functions are site-dependent, for instance, depending on the net CH_4 production characteristics of the site. In the simulation employing the linear root distribution function, model-derived pore water CH_4 concentration profiles underestimated field observations in the upper level of the
5 peat column (Fig. 12). The lower concentration was due to a poor representation of transport in the upper portion of the soil column when a linear root density function was used. Whereas the exponential distribution extended smoothly down into depth of the peat column and so did the pore water concentration when such a root distribution was used. Also, the pore water CH_4 concentrations were less satisfying when compared to
10 those from standard simulations. Therefore, based on our results, it is suggested that the exponential distribution is a superior representation of root density as a function of depth.

4 Conclusions

We revised an extant process-based biogeochemistry model, the Terrestrial Ecosys-
15 tem Model to account for the effects of multiple substances in a soil profile on CH_4 production, oxidation, and transport. The new development allows CH_4 effluxes to be modeled with different levels of model complexity. When four-substances (O_2, N_2, CO_2 and CH_4) are considered, the inhibitory effect of O_2 on CH_4 production and the stimulatory effect of O_2 on CH_4 oxidation are well accounted for, and ebullition is modeled
20 in a physically logical manner. When ebullition is modeled with a concentration-based threshold approach and when the inhibition effect of O_2 on CH_4 production are invoked, and when the competition for O_2 between methanotrophy and heterotrophic respiration are retained, the model becomes essentially a two-substance system. If we ignore the role of O_2, while modeling bubble ebullition with the concentration based threshold
25 function, the model is reduced to a one-substance system. These models were tested through a group of sensitivity analyses at two temperate peatland sites in Michigan. We showed that only the four-substance model with the new ebullition algorithm is able

Printer-friendly Version

Interactive Discussion

to account for the effects of a sudden drop in atmospheric pressure on the episodic emissions. All models simulated the retarding effect on CH_4 efflux after an increase in surface standing water due to inhibited diffusion and enhanced rhizospheric oxidation. We concluded that, to more accurately account for the effects of atmospheric pressure dynamics and water table dynamics on methane effluxes, the four-substance model with the probabilistic but physics-based ebullition algorithm should be used in the future to quantify global wetland CH_4 emissions. Further, to more accurately simulate the pore water gas concentrations and different pathways of CH_4 transport, an exponential root distribution function should be used and the phase-related parameters should be treated as temperature dependent.

Appendix A

The Henry's law constants (unit: $M\,atm^{-1}$) (Sander, 1999) are computed as

$$H = 6.1 \times 10^{-4} \exp\left[-1300\left(\frac{1}{T} - \frac{1}{298.0}\right)\right] \quad \text{for } N_2 \tag{A1}$$

$$H = 1.3 \times 10^{-3} \exp\left[-1500\left(\frac{1}{T} - \frac{1}{298.0}\right)\right] \quad \text{for } O_2 \tag{A2}$$

$$H = 3.4 \times 10^{-2} \exp\left[-2400\left(\frac{1}{T} - \frac{1}{298.0}\right)\right] \quad \text{for } CO_2 \tag{A3}$$

$$H = 1.3 \times 10^{-3} \exp\left[-1700\left(\frac{1}{T} - \frac{1}{298.0}\right)\right] \quad \text{for } CH_4 \tag{A4}$$

where T is temperature (unit: K).

The Bunsen coefficient or solubility for gas i is related to Henry's law constant as

$$\alpha_i = H_i \times \frac{T}{12.2} \tag{A5}$$

6141

The diffusivities (unit: $m^2\,s^{-1}$) (Frank et al., 1996; Arah and Stephen, 1998; Winkelmann, 2008) in air are computed as

$$D_a = 1.93 \times 10^{-5} \times \left(\frac{T}{273.0}\right)^{1.82} \quad \text{for } N_2 \tag{A6}$$

$$D_a = 1.8 \times 10^{-5} \times \left(\frac{T}{273.0}\right)^{1.82} \quad \text{for } O_2 \tag{A7}$$

$$D_a = 1.47 \times 10^{-5} \times \left(\frac{T}{273.15}\right)^{1.792} \quad \text{for } CO_2 \tag{A8}$$

$$D_a = 1.9 \times 10^{-5} \times \left(\frac{T}{298.0}\right)^{1.82} \quad \text{for } CH_4 \tag{A9}$$

The diffusivities (unit: $m^2\,s^{-1}$) in water are computed as

$$D_w = 2.57 \times 10^{-9} \times \left(\frac{T}{273.0}\right) \quad \text{for } N_2 \tag{A10}$$

$$D_w = 2.4 \times 10^{-9} \left(\frac{T}{298.0}\right) \quad \text{for } O_2 \tag{A11}$$

$$D_w = 1.81 \times 10^{-6} \exp\left(\frac{-2032.6}{T}\right) \quad \text{for } CO_2 \tag{A12}$$

$$D_w = 1.5 \times 10^{-9} \times \left(\frac{T}{298.0}\right) \quad \text{for } CH_4 \tag{A13}$$

Appendix B

The maximum CH_4 production potential is defined as

$$P^*_{CH_4} = \hat{P}_{CH_4} f(S_{OM}(z,t)) f(T(z,t)) f(pH(z,t)) f(Eh(z,t)) \tag{B1}$$

where $f(S_{OM}(z,t))$, $f(T(z,t))$, $f(pH(z,t))$, $f(Eh(z,t))$ are multiplier functions of methanogenesis substrate availability (modeled as a function of scaled NPP), soil temperature, pH value and redox potential, as defined in Zhuang et al. (2004). $\hat{P}_{CH_4}$ (unit: $mol\,m^{-3}\,s^{-1}$) is a scaling parameter for model calibration. Another site specific parameter that needs calibration is the Q_{10} coefficient ($P_{Q_{10}}$) of $f(T(z,t))$.

The maximum CH_4 oxidation potential is defined as

$$O^*_{CH_4} = \hat{O}_{CH_4} f(T(z,t)) f(\theta(z,t)) f(Eh(z,t)) \tag{B2}$$

where $f(T(z,t))$, $f(\theta(z,t))$, $f(Eh(z,t))$ are functions of soil temperature, soil moisture and redox potential (see Zhuang et al., 2004 for detailed descriptions). Parameter $\hat{O}_{CH_4}$ (unit: $mol\,m^{-3}\,s^{-1}$) is calibrated for every representative site. The Q_{10} coefficient for temperature effect is set to 2 throughout this study.

Appendix C

For the diffusive flux, the diffusion constant in Eq. (1) is defined for the bulk median, which is conventionally computed (Stephen et al., 1998) as

$$D_i = \frac{1}{\tau} \frac{\epsilon D_{i,a} + \alpha_i \theta D_{i,w}}{\epsilon + \alpha_i \theta} \tag{C1}$$

where subscripts a and w denote the diffusivity in air and in water (see Appendix A for ways of computation). τ is the tortuosity factor in the soil, taken as 1.5 throughout the study (Arah and Stephen, 1998).

For gas transport through the aerenchyma of wetland plants, we, following the argument in other studies (Teal and Kanwisher, 1966; Matthews et al., 2000; Segers and Leffelaar, 2001), assumed the N_2, CO_2 and CH_4 are transported in a similar way, such that

$$R_i = R_i^*(y_{i,\mathrm{a}} - y_{i,\mathrm{atm}}) = \lambda_r L_v D_{i,\mathrm{a}} f(t)(y_{i,\mathrm{a}} - y_{i,\mathrm{atm}}) \tag{C2}$$

where λ_r (unit: m air (m root)$^{-1}$) is the specific conductivity of the root system and L_v (unit: m root m^{-3} soil) is the root length density. A value of 3.0×10^{-4} was used for λ_r. The vertical distribution of L_v in soil is assumed following the Gale-Grigal model (Jackson et al., 1996) (see the exponential model in Appendix D). The temporal variation $f(t)$ of the root is modeled similarly to Zhuang et al. (2004) and Walter and Heimann (2000). Also, we assumed the four gases can either be transported from the atmosphere to the roots or from the roots to the atmosphere. When the one-substance model is switched on, the oxidation of CH_4 in the rhizosphere (Beckett et al., 2001) is not considered explicitly, rather, as in Walter and Heimann (2000), we assume 50% of CH_4 is oxidized.

In the S4 model, the governing equation for CH_4 is

$$\frac{\partial y_{CH_4}}{\partial t} = \frac{\partial}{\partial z}\left(D_{CH_4}\frac{\partial y_{CH_4}}{\partial z}\right) + \frac{P_{CH_4}^*}{1 + \eta y_{O_2,\mathrm{w}}}$$
$$-Q_{CH_4}^* \frac{y_{CH_4,\mathrm{w}}}{k_{CH_4} + y_{CH_4,\mathrm{w}}}\frac{y_{O_2,\mathrm{w}}}{k_{O_2} + y_{O_2,\mathrm{w}}} - E_{CH_4} + R_{CH_4}^*\left(y_{CH_4,\mathrm{atm}} - y_{CH_4,\mathrm{a}}\right) \tag{C3}$$

for CO_2 is

$$\frac{\partial y_{CO_2}}{\partial t} = \frac{\partial}{\partial z}\left(D_{CO_2}\frac{\partial y_{CO_2}}{\partial z}\right) + \frac{P_{CH_4}^*}{1 + \eta y_{O_2,\mathrm{w}}} + Q_{CH_4}^* \frac{y_{CH_4,\mathrm{w}}}{k_{CH_4} + y_{CH_4,\mathrm{w}}}\frac{y_{O_2,\mathrm{w}}}{k_{O_2} + y_{O_2,\mathrm{w}}}$$
$$+V_R^* \frac{y_{O_2,\mathrm{w}}}{k_R + y_{O_2,\mathrm{w}}} - E_{CO_2} + R_{CO_2}^*\left(y_{CO_2,\mathrm{atm}} - y_{CO_2,\mathrm{a}}\right) \tag{C4}$$

Methane emission modeling

J. Tang et al.

for O_2 is

$$\frac{\partial y_{O_2}}{\partial t} = \frac{\partial}{\partial z}\left(D_{O_2}\frac{\partial y_{O_2}}{\partial z}\right) - 2Q^*_{CH_4}\frac{y_{CH_4,w}}{k_{CH_4}+y_{CH_4,w}}\frac{y_{O_2,w}}{k_{O_2}+y_{O_2,w}} - V^*_R\frac{y_{O_2,w}}{k_R+y_{O_2,w}}$$

$$-E_{O_2} + R^*_{O_2}\left(y_{O_2,atm} - y_{O_2,a}\right) \tag{C5}$$

and for N_2 is

$$\frac{\partial y_{N_2}}{\partial t} = \frac{\partial}{\partial z}\left(D_{N_2}\frac{\partial y_{N_2}}{\partial z}\right) - E_{N_2} + R^*_{N_2}\left(y_{N_2,atm} - y_{N_2,a}\right) \tag{C6}$$

Appendix D

The root length density in Eq. (C2) is defined as

$$L_v = R_{veg}f(z) = -R_{veg} \times 100\log(\beta)\beta^{100z} \tag{D1}$$

where β is 0.943 for Buck Hollow Bog, and 0.910 for Big Cassandra Bog. And R_{veg} is a scaling parameter needs calibration to account for differences in conducting capabilities for different plants. Note, the integrated root distribution function $f(z)$ from lower boundary to soil surface equals one. The alternative root distribution used in Sect. 3.4, is defined as

$$f(z) = \begin{array}{ll} \frac{2}{R_d}\left(1-\frac{z}{R_d}\right) & \text{for } 0 \leq z \leq R_d \\ 0 & \text{otherwise} \end{array} \tag{D2}$$

where R_d is root depth, computed using the Gale-Grigal model. This is different from the formula adopted in Walter and Heimann (2000) and Zhuang et al. (2004) and that we here imposed the constraint such that the vertical integration of $f(z)$ equals one.

6145

Symbol	Definition
α_i	Bunsen coefficient for substance i, unitless.
β	coefficient for root distribution, unitless.
$\delta(s)$	Dirac delta function
$\epsilon(z,t)$	air-filled porosity, unit: m^3 air m^{-3} soil.
η	inhibition coefficient of O_2 on methanogenesis, unit: $m^3\,mol^{-1}$.
$\theta(z,t)$	soil moisutre, unit: m^3 water m^{-3} soil.
λ_r	specific conductivity of the root system, unit: m air m^{-1} root.
τ	tortuosity factor in the soil, unitless.
b	pressure imposed by water column above water table ($z_{wt} < 0$) or soil surface ($z_{wt} \geq 0$), unit: m.
$CH_{4,max}$	threshold concentration for CH_4 ebullition, unit: $mol\,m^{-3}$ water.
D_i	bulk diffusivity of substance i in soil, unit: $m^2\,s^{-1}$.
$D_{i,a}$	diffusivity of substance i in air, unit: $m^2\,s^{-1}$.
$D_{i,w}$	diffusivity of substance i in water, unit: $m^2\,s^{-1}$.
$E(z)$	total ebullition of the gases at depth z, unit: $mol\,m^{-2}$.
$Eb_i(z)$	potential ebullition of gas i at depth z, unit: $mol\,m^{-2}$.
H_i	Henry's law constant for substance i, unit: $M\,atm^{-1}$.
k_{CH_4}	Michaelis-Menten coefficient for CH_4, unit: $mol\,m^{-3}$ water.
k_{O_2}	Michaelis-Menten coefficient for O_2, unit: $mol\,m^{-3}$ water.
k_R	Michaelis-Menten coefficient for respiration, unit: $mol\,m^{-3}$ water.
L_v	root length density, unit: m root m^{-3} soil.
$O_{2,max}$	threshold concentration for O_2 ebullition, unit: $mol\,m^{-3}$ water.
p	atmospheric pressure, unit: Pa.
$P^*_{CH_4}$	maximum CH_4 production potential, unit: $mol\,m^{-3}\,s^{-1}$.
P_{OX}	fraction of CH_4 oxidized in rhizosphere, unitless.

Full Screen / Esc

Printer-friendly Version

Interactive Discussion

$P_{Q_{10}}$	Q_{10} coefficient for methanogenesis, unitless.
p_r	probability of bubble redissolution, unitless.
$P_s(z,t)$	total gas pressure at depth z, time t, unit: Pa.
$P_{s,i}(z,t)$	partial gas pressure at depth z, time t by substance i, unit: Pa.
P_0	pressure scaling factor, unit: Pa.
$\hat{p}$	scaled atmospheric pressure, unitless.
$Q^*_{CH_4}$	maximum CH_4 oxidation potential, unit: $mol\,m^{-3}\,s^{-1}$.
R^*_i	scaled rate of plant aided transport, unit: s^{-1}
R_d	root depth, unit: m.
R_{veg}	vegetation type dependent scaling parameter of gas conducting capability, unitless.
V^*_R	maximum rate of respiration, unit: $mol\,m^{-3}\,s^{-1}$.
y_i	bulk concentration of substance i, unit: $mol\,m^{-3}$.
$y_{i,a}$	gaseous concentration of substance i, unit: $mol\,m^{-3}$ air.
$y_{i,w}$	aqueous concentration of substance i, unit: $mol\,m^{-3}$ water.
$y_{i,atm}$	concentration of substance i in the atmosphere, unit: $mol\,m^{-3}$ air.
$\tilde{y}_i$	equilibrium bulk concentration of substance i, unit: $mol\,m^{-3}$.
$\tilde{y}_{i,w}$	equilibrium aqueous concentration of substance i, unit: $mol\,m^{-3}$ water.
z_{wt}	depth of water table, unit: m.
z_s	depth of soil surface, unit: m.
z_0	water depth scaling factor, unit: m.
Z	depth of lower boundary, unit: m.

References

Arah, J. R. M. and Kirk, G. J. D.: Modeling rice plant-mediated methane emission, Nutr. Cycl. Agroecosys., 58, 221–230, 2000. 6123, 6127, 6128, 6129

Arah, J. R. M. and Stephen, K. D.: A model of the processes leading to methane emission from peatland, Atmos. Environ., 32, 3257–3264, 1998. 6142, 6143

Baird, A. J., Beckwith, C. W., Waldron, S., and Waddington, J. M.: Ebullition of methane-containing gas bubbles from near-surface Sphagnum peat, Geophys. Res. Lett., 31, doi:10.1029/2004GL021157, 2004. 6124, 6131

Bazhin, N. M.: Gas transport in a residual layer of a water basin, Chemosphere-Global Change Science, 3, 33–40, 2001. 6124, 6129

Bazhin, N. M.: Influence of plants on the methane emission from sediments, Chemosphere, 54, 209–215, 2004. 6124, 6129

Beckett, P. M., Armstrong, W., and Armstrong, J.: Mathematical modeling of methane transport by Phragmites: the potential for diffusion within the roots and rhizosphere, Aquat. Bot., 69, 293–312, 2001. 6144

Cao, M., Dent, J. B., and Heal, O. W.: Modeling methane emissions from rice paddies, Global Biogeochem. Cy., 9, 183–195, 1995. 6124

Conrad, R.: Control of Methane Production in Terrestrial Ecosystems, J. Wiley & Sons, New York, NY, USA, 1989. 6126, 6128

Coulthard, T. J., Baird, A. J., Ramirez, J., and Waddington, J. M.: Methane Dynamics in Peat: Importance of Shallow Peats and a Novel Reduced-Complexity Approach for Modeling Ebullition, AGU, Washington, DC, USA, 2009. 6124

Denman, K., Brasseur, G., Chidthaisong, A., Ciais, P., Cox, P., Dickinson, R. E., Hauglustaine, D., Heinze, C., Holland, E., Jacob, D., Lohmann, U., Ramachandran, S., da Silva Dias, P. L., Wofsy, S. C., and Zhang, X.: Coupling between changes in the climate system and biogeochemistry, in: Climate Change 2007: The Physical Science Basis. Contribution of Working Group I to the Fourth Assessment Report of the Intergovernmental Panel on Climate Change, edited by: Solomon, S., Qin, D., Manning, M., Chen, Z., Marguis, M., Avery, K., Tignor, M., and Hiller, M., Cambridge University Press, UK and New York, NY, USA, 2007. 6123

Forster, P., Ramaswamy, V., Artaxo, P., Berntsen, T., Betts, R., Fahey, D., Haywood, J., Lean, J., Lowe, D., Myhre, G., Nganga, J., Prinn, R., Raga, G., Schulz, M., and Dorland, R. V.:

Changes in atmospheric constituents and in radiative forcing, in: Climate Change 2007: The Physical Science Basis. Contribution of Working Group I to the Fourth Assessment Report of the Intergovernmental Panel on Climate Change, edited by: Solomon, S., Qin, D., Manning, M., Chen, Z., Marguis, M., Avery, K., Tignor, M., and Hiller, M., Cambridge University Press, UK and New York, NY, USA, 2007. 6133

Frank, M. J. W., Kuipers, J. A. M., and van Swaaij, W. P. M.: Diffusion coefficients and viscosities of CO_2+H_2O, CO_2+CH_3OH, NH_3+H_2O and NH_3+CH_3OH liquid mixtures, J. Chem. Eng. Data, 41, 297–302, 1996. 6142

Jackson, R. B., Canadell, J., Ehleringer, J. R., Mooney, H. A., Sala, O. E., and Schulze, E. D.: A global analysis of root distributions for terrestrial biomes, Oecologia, 108, 389–411, 1996. 6139, 6144

Kellner, E., Baird, A. J., Oosterwoud, M., Harrison, K., and Waddington, J. M.: Effect of temperature and atmospheric pressure on methane (CH_4) ebullition from near-surface peats, Geophys. Res. Lett., 33, doi:10.1029/2006GL027509, 2006. 6124, 6130, 6131

Martens, C. and Klump, J. V.: Biogeochemical cycling in an organic-rich coastal marine basin-1. Methane sediment-water exchange processes, Geochim. Cosmochim. Ac., 44, 471–490, 1980. 6124, 6130

Matthews, R. B., Wassmann, R., and Arah, J.: Using a crop/soil simulation model and GIS techniques to assess methane emissions from rice fields in Asia. I. Model development, Nutr. Cycl. Agroecosys., 58, 141–159, 2000. 6124, 6128, 6144

Mattson, M. D. and Likens, G. E.: Air pressure and methane fluxes, Nature, 347, 718–719, 1990. 6124

Mitchell, T. D., Carter, T. R., Jones, P. D., Hulme, M., and New, M.: A comprehensive set of high-resolution grids of monthly climate for Europe and the globe: the observed record (1901–2000) and 16 scenarios (2001–2100), Tyndall Center Working Paper 55, University of East Anglia, Norwich, UK, July, 25 pp., 2004. 6133

Oleson, K. W., Dai, Y., Bonan, G., Bosilovich, M., Dickinson, R., Dirmeyer, P., Hoffman, F., Houser, P., Levis, S., Niu, G., Thornton, P., Vertenstein, M., Yang, Z., and Zeng, X.: Technical description of he community land model (CLM), Tech. rep., Terrestrial Science Section, Climate and Global Dynamics Division, National Center for Atmospheric Research, Boulder, Colorado, USA, 2004. 6132

Peck, A. J.: The water table as affected by atmospheric pressure, J. Geophys. Res., 65, 2383–2388, 1960. 6129

Methane emission modeling

J. Tang et al.

Potter, C. S.: An ecosystem simulation model for methane production and emission from wetlands, Global Biogeochem. Cy., 11, 495–506, 1997. 6124

Rosenberry, D. O., Glaser, P. H., Siegel, D. I., and Weeks, E. P.: Use of hydraulic head to estimate volumetric gas content and ebullition flux in northern peatlands, Water Resour. Res., 39, doi:10.1029/2002WR001377, 2003. 6129

Rothfuss, F. and Conrad, R.: Effect of gas bubbles on the diffusive flux of methane in anoxic paddy soil, Limnol. Oceanogr., 43, 1511–1518, 1998. 6132

Sander, R.: Compilation of Henry's law constants for inorganic and organic species of potential importance in environmental chemistry (version 3), http://www.mpch-mainz.mpg.de/~sander/res/henry.html, 1999. 6141

Sass, R. L., Fisher Jr., M. F., and Huang, Y.: A process-based model for methane emissions from irrigated rice fields: experimental basis and assumptions, Nutr. Cycl. Agroecosys., 58, 249–258, 2000. 6124

Schiesser, W. E.: The Numerical Method of Lines: Integration of Partial Differential Equations, Academic Press, San Diego, 1991. 6132

Segers, R. and Leffelaar, P. A.: Modeling methane fluxes in wetlands with gas-transporting plants, 1. Single-root scale, J. Geophys. Res., 106, 3511–3528, 2001. 6128, 6144

Shannon, R. D. and White, J. R.: A three-year study of controls on methane emissions from two Michigan peatlands, Biogeochemistry, 27, 35–60, 1994. 6133, 6135

Shannon, R. D., White, J. R., Lawson, J. E., and Gilmour, B. S.: Methane efflux from emergent vegetation in peatlands, J. Ecol., 84, 239–246, 1996. 6137

Stephen, K. D., Arah, J. R. M., Daulat, W., and Clymo, R. S.: Root-mediated gas transport in peat determined by argon diffusion, Soil Biol. Biochem., 30, 501–508, 1998. 6143

Teal, J. M. and Kanwisher, J. W.: Gas transport in the marsh grass, *Spartina alterniflora*, J. Exp. Bot., 17, 355–361, 1966. 6144

Tokida, T., Miyazaki, T., and Mizoguchi, M.: Ebullition of methane from peat with falling atmospheric pressure, Geophys. Res. Lett., 32, doi:10.1029/2005GL022949, 2005. 6124

Tokida, T., Miyazaki, T., Mizoguchi, M., Nagata, O., Takakai, F., Kagemoto, A., and Hatano, R.: Falling atmospheric pressure as a trigger for methane ebullition from peatland, Global Biogeochem. Cy., 21, doi:10.1029/2006GB002790, 2007. 6124, 6128, 6129

van Bodegom, P., Goudriaan, J., and Leffelaar, P.: A mechanistic model on methane oxidation in a rice rhizosphere, Biogeochemistry, 55, 145–177, 2001. 6128

van Huissteden, J., van den Bos, R., and Alvarez, I. M.: Modeling the effect of water table

management on CO_2 and CH_4 from peat soils, Neth. J. Geosci., 85, 3–18, 2006. 6123, 6139

Walter, B. P. and Heimann, M.: A process-based, climate-sensitive model to derive methane emissions from natural wetlands: application to five wetland sites, sensitivity to model parameters, and climate, Global Biogeochem. Cy., 14, 745–765, 2000. 6123, 6124, 6129, 6132, 6133, 6139, 6144, 6145

Walter, B. P., Heimann, M., and Matthews, E.: Modeling modern methane emissions from natural wetlands, 1. Model description and results, J. Geophys. Res., 106, 34189–34206, 2001. 6123, 6127

Wania, R., Ross, I., and Prentice, I. C.: Implementation and evaluation of a new methane model within a dynamic global vegetation model: LPJ-WHyMe v1.3, Geosci. Model Dev. Discuss., 3, 1–59, doi:10.5194/gmdd-3-1-2010, 2010. 6130, 6131

Winkelmann, J.: Diffusion of carbon dioxide(1); water(2); sodium chloride(3), in: Gases in Gases, Liquids and their Mixtures, edited by: Lechner, M., Springer, Berlin Heidelberg, 2273–2274, 2008. 6142

Zhang, Y., Li, C., Trettin, C. C., Li, H., and Sun, G.: An integrated model of soil, hydrology, and vegetation for carbon dynamics in wetland ecosystems, Global Biogeochem. Cy., 16, doi:10.1029/2001GB001838, 2002. 6124

Zhuang, Q., Mellilo, J. M., Kicklighter, D. W., Prinn, R. G., McGuire, A. D., Steudler, P. A., Felzer, B. S., and Hu, S.: Methane fluxes between terrestrial ecosystems and the atmosphere at northern high latitudes during the past century: a retrospective analysis with a process-based biogeochemistry model, Global Biogeochem. Cy., 18, doi:10.1029/2004GB002239, 2004. 6123, 6124, 6125, 6127, 6129, 6131, 6133, 6139, 6143, 6144, 6145

Zhuang, Q., Melack, J. M., Zimov, S., Walter, K. M., Butenhoff, C. L., and Khalil, M. A. K.: Global methane emissions from wetlands, rice paddies and lakes, Trans. Am. Geophys. Union (EOS), 37–38, 90, 2009. 6123

Zona, D., Oechel, W. C., Kochendorter, J., U, Paw U, K. T., Salyuk, A. N., Olivas, P. C., Oberbauer, S. F., and Lipson, D. A.: Methane fluxes during the initiation of a large-scale water table manipulation experiment in the Alaskan Arctic tundra, Global Biogeochem. Cy., 23, doi:10.1029/2009GB003487, 2009. 6125, 6128

Title Page

Abstract | Introduction

Conclusions | References

Tables | Figures

◀ | ▶

◀ | ▶

Back | Close

Full Screen / Esc

Printer-friendly Version

Interactive Discussion

Table 1. Parameters calibrated for standard model simulations.

	$\hat{P}_{CH_4}$ $(\mathrm{mol\,m^{-3}\,s^{-1}})$	$P_{Q_{10}}$ (None)	$\hat{O}_{CH_4}$ $(\mathrm{mol\,m^{-3}\,s^{-1}})$	R_{veg} (None)
Buck Hollow site				
S1-model	3.5×10^{-7}	12.7	1.10×10^{-7}	1.2×10^{-3}
S2-model	2.5×10^{-6}	12.7	1.10×10^{-8}	1.2×10^{-3}
S4-model	1.25×10^{-6}	12.7	1.10×10^{-8}	1.2×10^{-3}
Big Cassandra site				
S1-model	7.5×10^{-8}	6	1×10^{-7}	1×10^{-3}
S2-model	2.75×10^{-6}	6	5×10^{-8}	1×10^{-3}
S4-model	1.375×10^{-6}	6	1×10^{-7}	1×10^{-3}

Table 2. Comparison of CH_4 efflux from the standard simulations to the measurements at the two Michigan peatlands. All statistics were tested for significance and were found significant with $p < 0.001$.

	Slope (None)	Intercept (mg CH_4 m^{-2} d^{-1})	RMSE (mg CH_4 m^{-2} d^{-1})	R^2 (None)
Buck Hollow site				
S1-model	0.79	83.5	165.1	0.51
S2-model	0.65	50.1	168.6	0.60
S4-model	0.84	68.0	154.5	0.55
Big Cassandra site				
S1-model	0.31	15.9	86.6	0.13
S2-model	0.52	−1.0	74.5	0.27
S4-model	0.78	−10.8	61.2	0.31

Methane emission modeling

J. Tang et al.

Table 3. Parameters calibrated for model simulations using a linear root distribution function.

	$\hat{P}_{CH_4}$ (mol m^{-3} s^{-1})	$P_{Q_{10}}$ (None)	$\hat{O}_{CH_4}$ (mol m^{-3} s^{-1})	R_{veg} (None)
Buck Hollow site				
S1-model	3.0×10^{-8}	12.7	1.10×10^{-7}	4.0×10^{-2}
S2-model	2.0×10^{-6}	12.7	1.10×10^{-8}	4.0×10^{-2}
S4-model	7.5×10^{-7}	12.7	1.10×10^{-8}	4.0×10^{-2}
Big Cassandra site				
S1-model	5.0×10^{-8}	6	1×10^{-7}	1.5×10^{-3}
S2-model	1.5×10^{-6}	6	5×10^{-8}	1.5×10^{-3}
S4-model	5.0×10^{-7}	6	1×10^{-7}	1.5×10^{-3}

Table 4. Comparison of CH_4 efflux from the simulations using a linear root distribution function to the measurements at the two Michigan peatlands. All statistics were tested for significance and were found significant with $p < 0.001$, except those denoted in the brackets.

	Slope (None)	Intercept (mg CH_4 m^{-2} d^{-1})	RMSE (mg CH_4 m^{-2} d^{-1})	R^2 (None)
Buck Hollow site				
S1-model	1.21	54.9	154.1	0.66
S2-model	0.78	47.9	139.8	0.64
S4-model	0.68	127.6	216.6	0.22
Big Cassandra site				
S1-model	0.10	32.1	103.7	0.19 ($p = 0.2$)
S2-model	0.10	26.5	183.6	0.07 ($p < 0.01$)
S4-model	0.27	13.2	104.6	0.14

```
(1) Initialize the total bubble flux E to zero
(2) DO l = N, N0, −1
(3) Compute potential bubble flux Eb at layer l
      IF Eb <= 0 .AND. E = 0 THEN
        GOTO step(2)
      ELSE
        IF Eb >= 0 THEN
(4)        Combine the bubbles, E=E+Eb
        ELSE
(5)        Draw a random number u from uniform distribution U[0,1]
          IF u <= abs(Eb)/(abs(Eb)+E) THEN
            IF abs(Eb) <= E THEN
(6)            Dissolve bubbles to make equality in Eq.(14) hold at layer l,
              and update, E=E−abs(Eb)
            ELSE
(7)            Dissolve bubbles with the amount E, thus E=0
            ENDIF
          ENDIF
        ENDIF
      ENDIF
    ENDIF
    ENDDO
(8) Release E to the atmosphere or add directly to the soil layer that is right above
 the water table.
Here, N is node ID of the bottom layer of the computation grids, and N0 is node ID
of the water table.
```

Fig. 1. The probabilistic algorithm used in S4 model to compute ebullition.
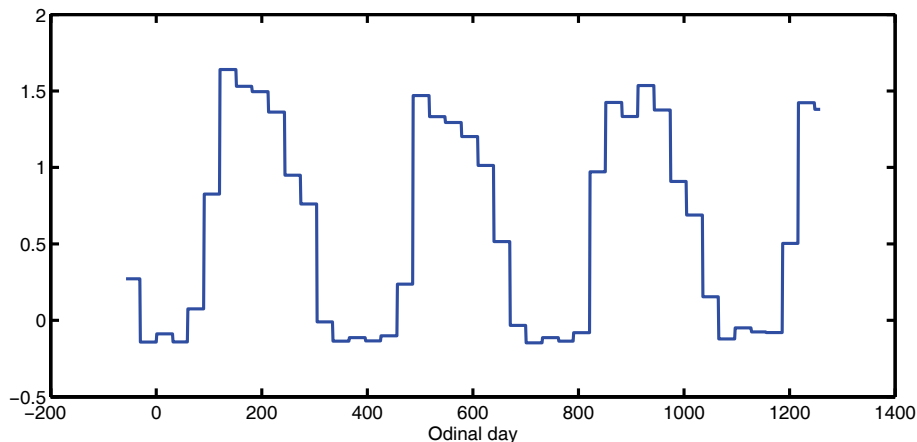
Fig. 2. The time series of scaled NPP (scaled with the median peak NPP at the site from a 100 year simulations) used as driving data in this study. Same data were used at both sites, with truncation into proper time periods.
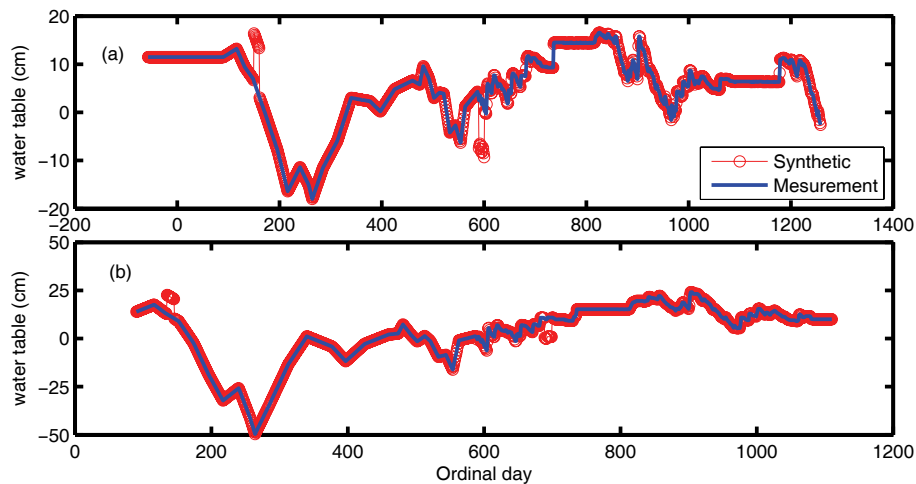
Fig. 3. The time series of water table depth used as driving data in this study at: **(a)** Buck Hollow site; **(b)** Big Cassandra site.
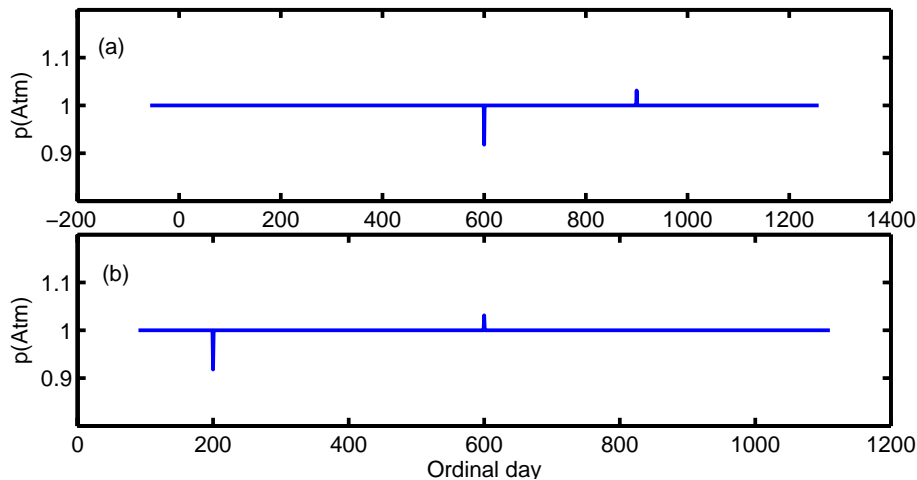
Fig. 4. Synthetic atmospheric pressure used in simulations for sensitivity analysis at: **(a)** Buck Hollow site; **(b)** Big Cassandra site.
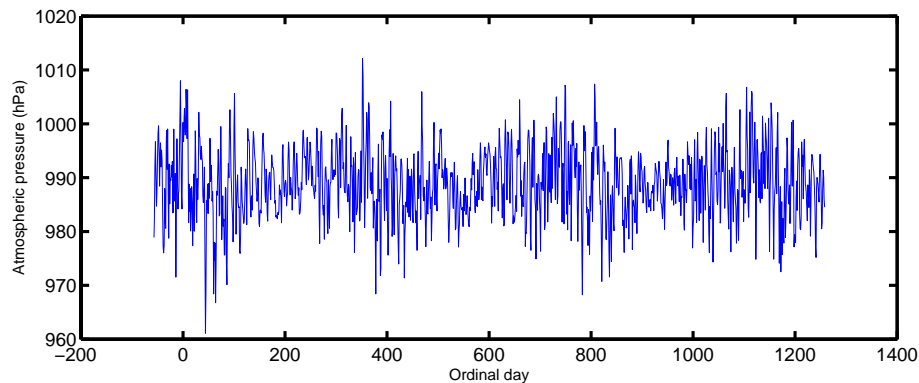
Fig. 5. Transient atmospheric pressure used in simulations for sensitivity analysis. Same time series was applied at both sites, with truncation into proper time periods.
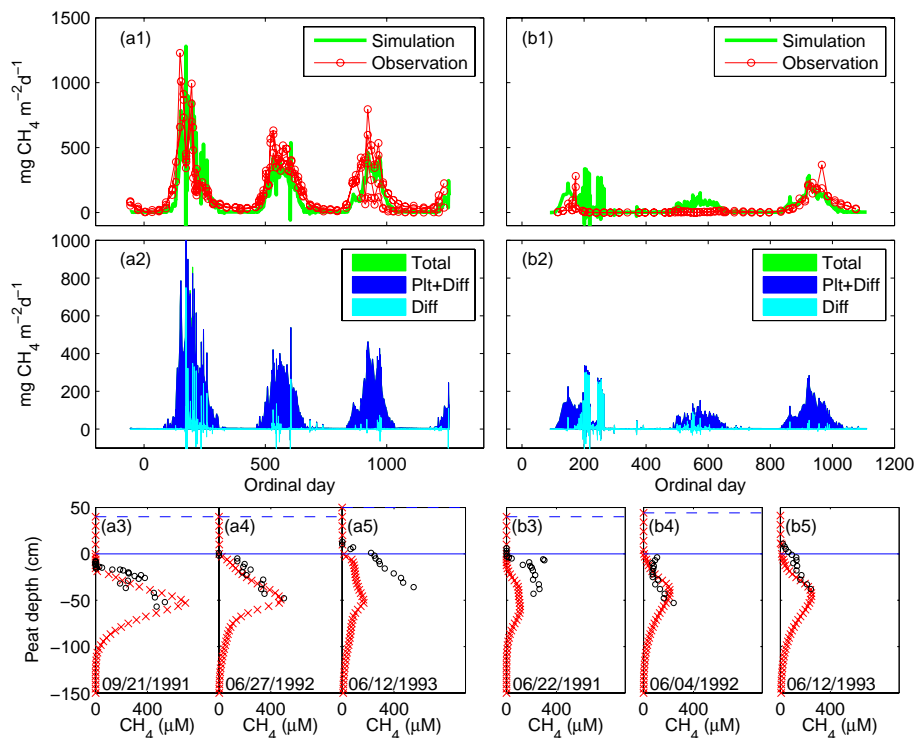
Fig. 6a. Methane effluxes, component-wise emissions and pore water concentration profiles from one-substance model (S1 model) in the standard simulations. **(a)** Panels for the Buck Hollow site. **(b)** Panels for the Big Cassandra site. Dashed lines indicate the level of water tables.
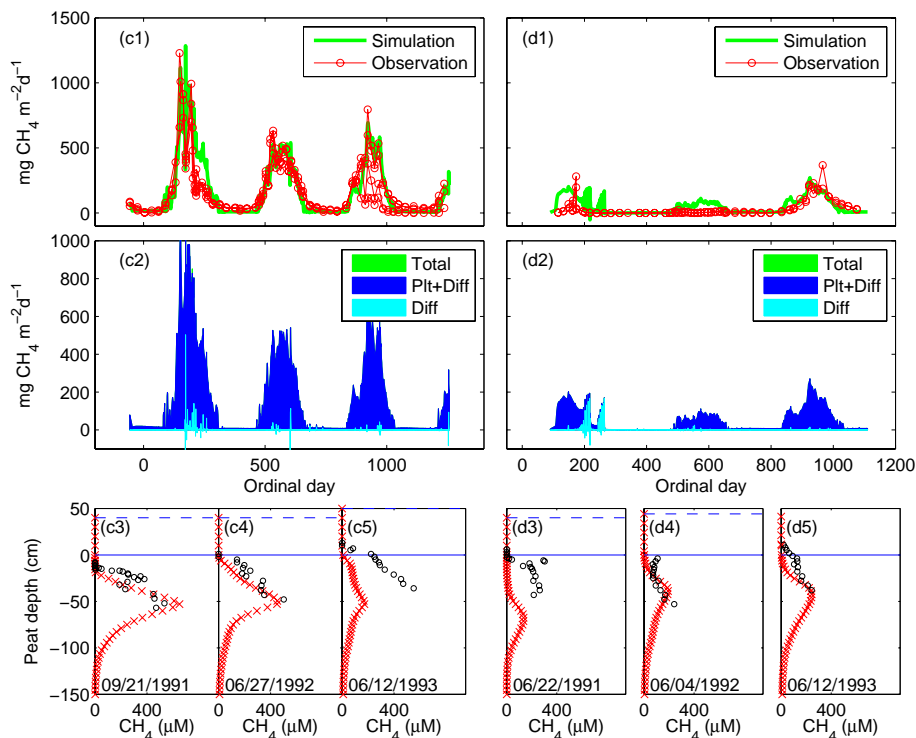
Fig. 6b. Methane effluxes, component-wise emissions and pore water concentration profiles from two-substance model (S2 model) in the standard simulations. **(c)** Panels for the Buck Hollow site. **(d)** Panels for the Big Cassandra site. Dashed lines indicate the level of water tables.
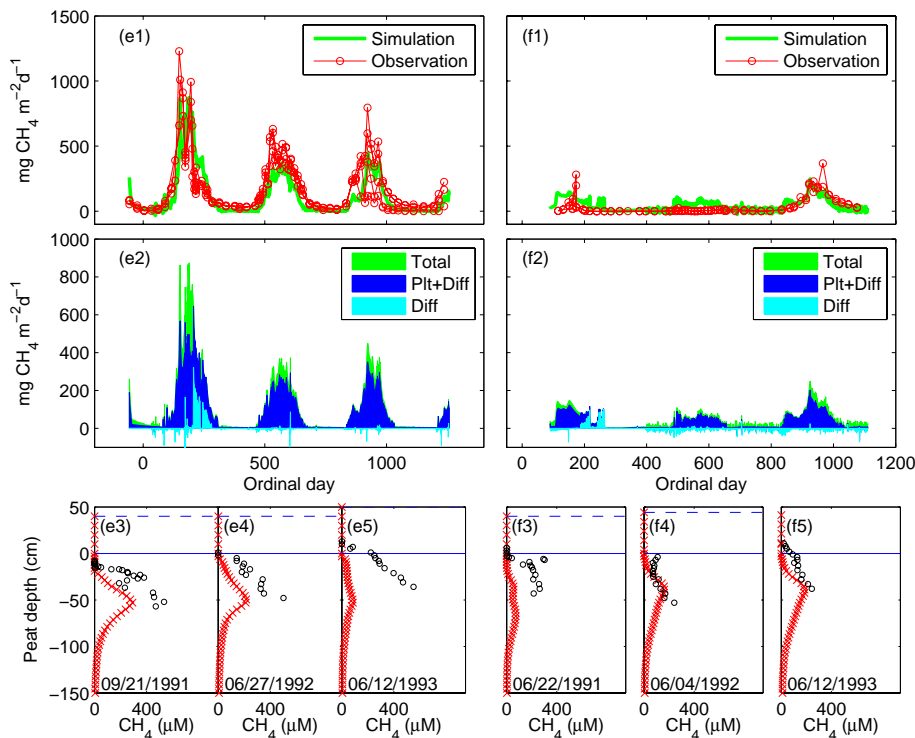
Fig. 6c. Methane effluxes, component-wise emissions and pore water concentration profiles from four-substance model (S4 model) in the standard simulations. **(e)** Panels for the Buck Hollow site. **(f)** Panels for the Big Cassandra site. Dashed lines indicate the level of water tables.
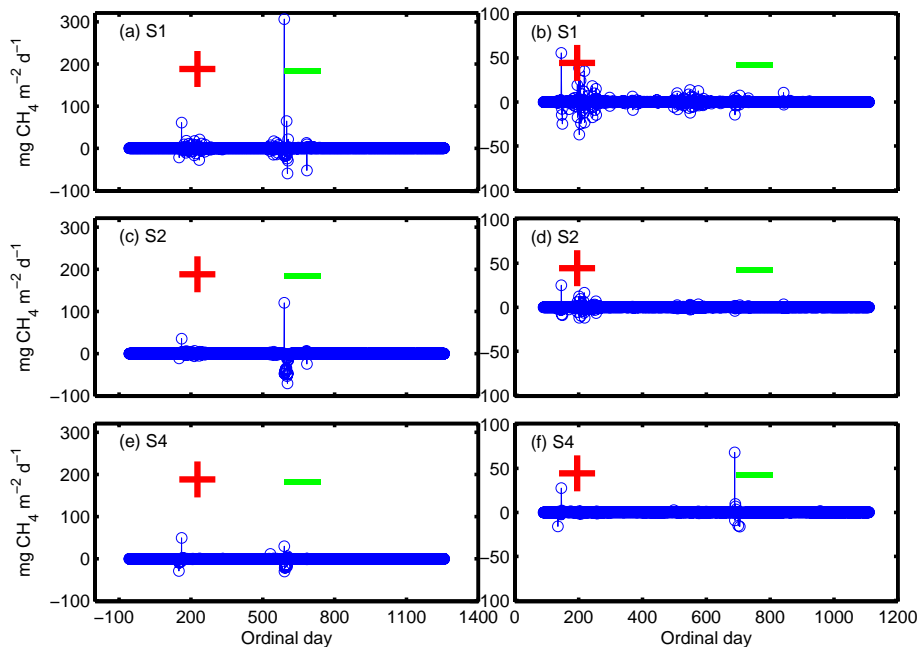
Fig. 7. Water table sensitivities with models of different complexities. Left-hand panels are for Buck Hollow site; right-hand panels are for Big Cassandra site. The red symbol "+" indicates the period of artificially increased water table depth, and the green symbol "−" indicates the period of artificially decreased water table depth.

Full Screen / Esc

Printer-friendly Version

Interactive Discussion
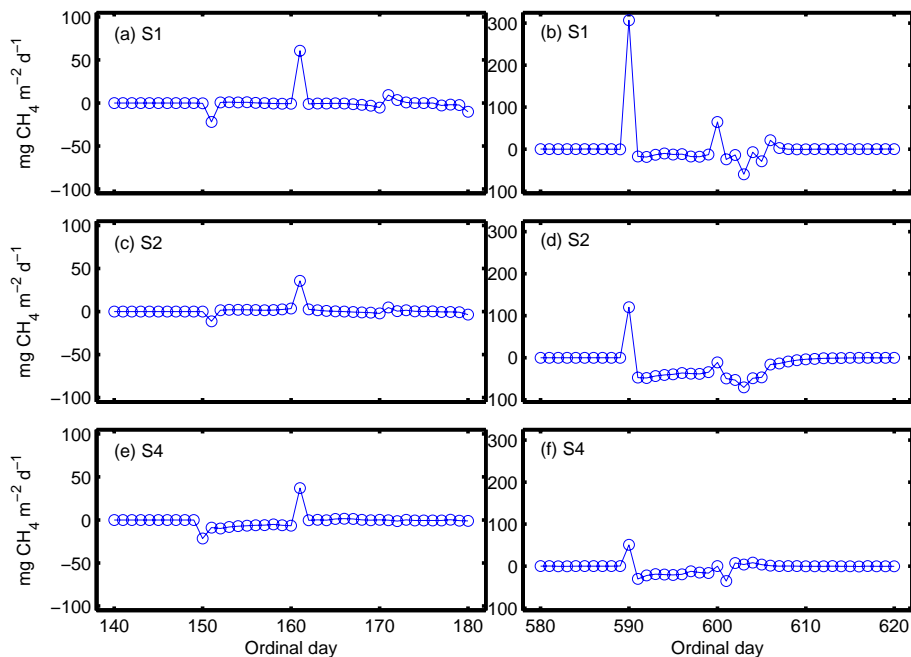
Fig. 8. Zoom-in plots for the water table sensitivity with models of different complexities at the Buck Hollow site. Left-hand panels were for the period where the water table depth is increased by 10 cm compared to the measured data, right-hand panels are for the period where the water table depth is decreased by 10 cm.
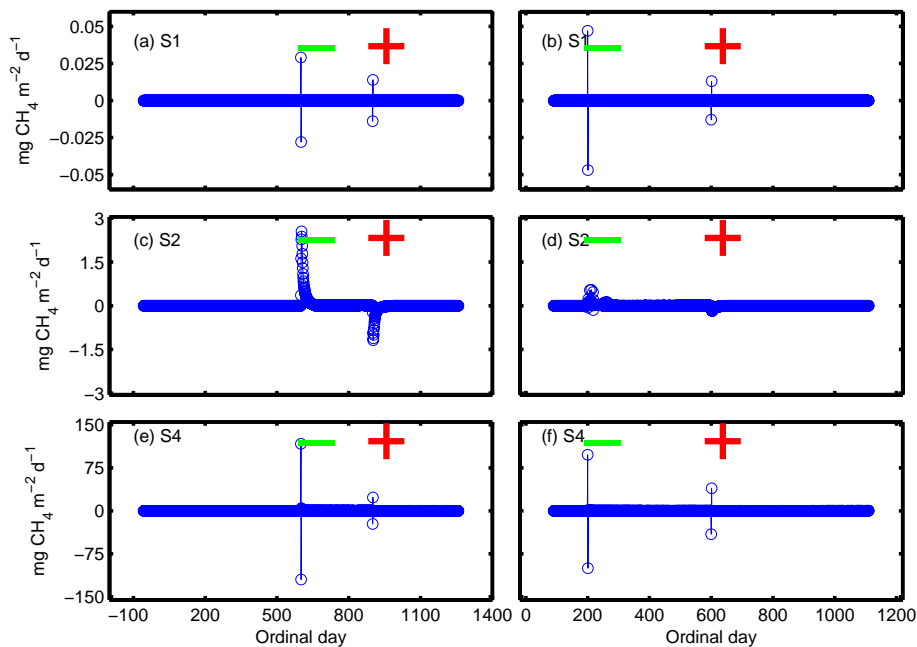
Fig. 9. Atmospheric pressure sensitivities with models of different complexities. **(a)**, **(c)** and **(e)** panels are for Buck Hollow site; **(b)**, **(d)** and **(f)** panels are for Big Cassandra site. The red symbol "+" indicates the day of artificially perturbed high pressure event, and the green symbol "−" indicates the day of artificially perturbed low pressure event. Note the scale of results from S4 model is 10^2 of that from S2 model, and 10^3 of that from S1 model.

Discussion Paper | Discussion Paper | Discussion Paper | Discussion Paper |

BGD

7, 6121–6171, 2010

Methane emission modeling
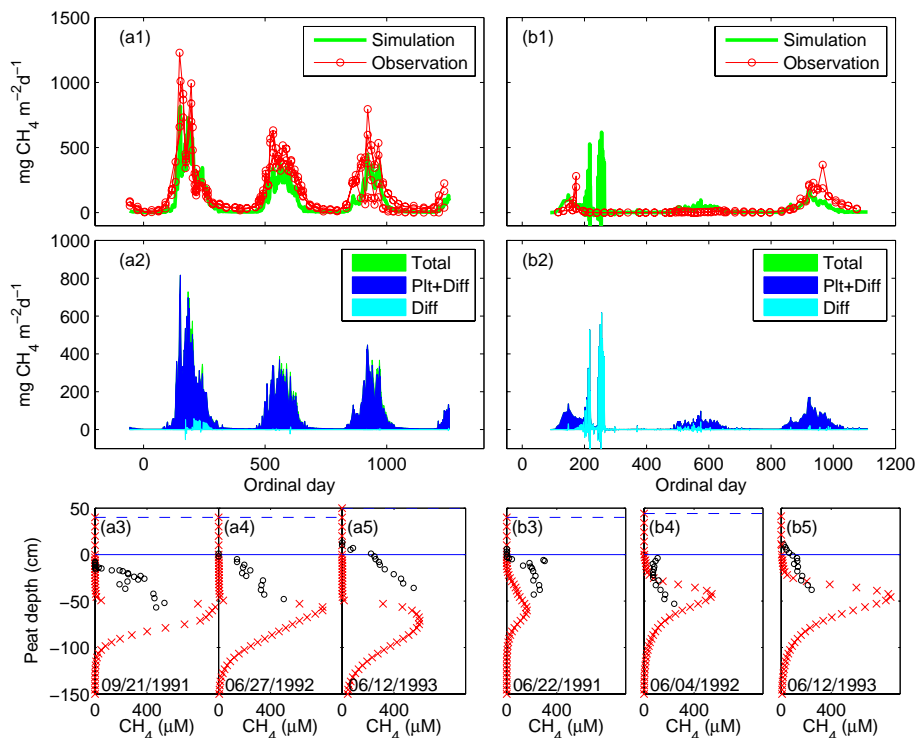
J. Tang et al.

Title Page

Abstract | Introduction

Conclusions | References

Tables | Figures

|◄ | ►|

◄ | ►

Back | Close

Full Screen / Esc

Printer-friendly Version

Interactive Discussion
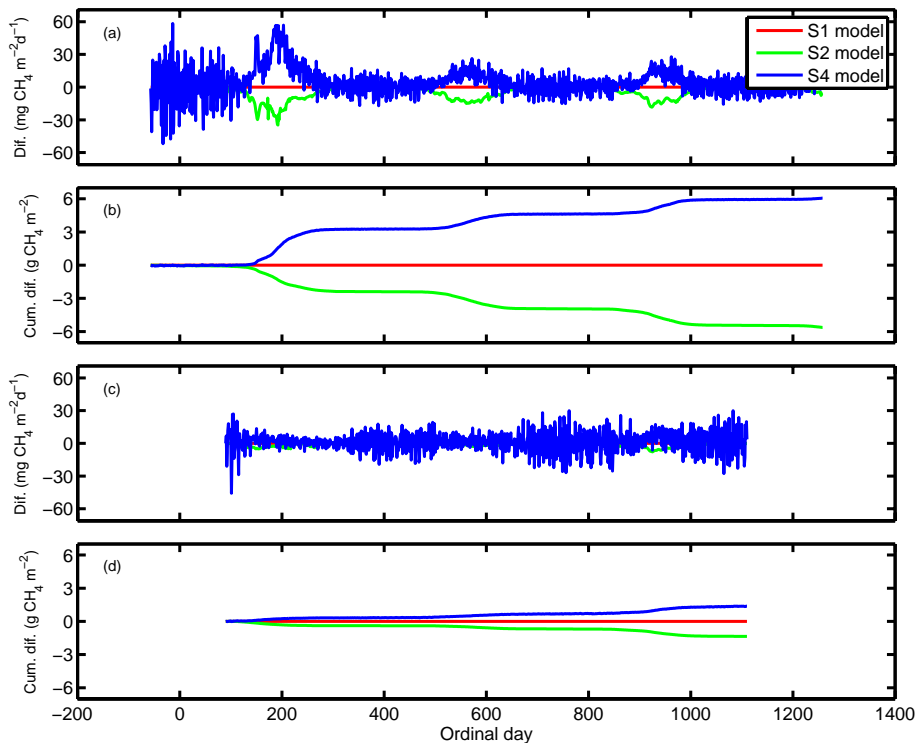
Fig. 10. Differences in the response to transient atmospheric pressure and that to constant atmospheric pressure with models of different complexities. **(a)** Time series of the absolute difference at the Buck Hollow site. **(b)** Time series of cumulative difference at the Buck Hollow site. **(c)** Time series of the absolute difference at the Big Cassandra site. **(d)** Time series of cumulative difference at the Big Cassandra site. The difference is defined by subtracting the fluxes simulated with the standard 1 atm pressure from that using the transient atmospheric pressure data.
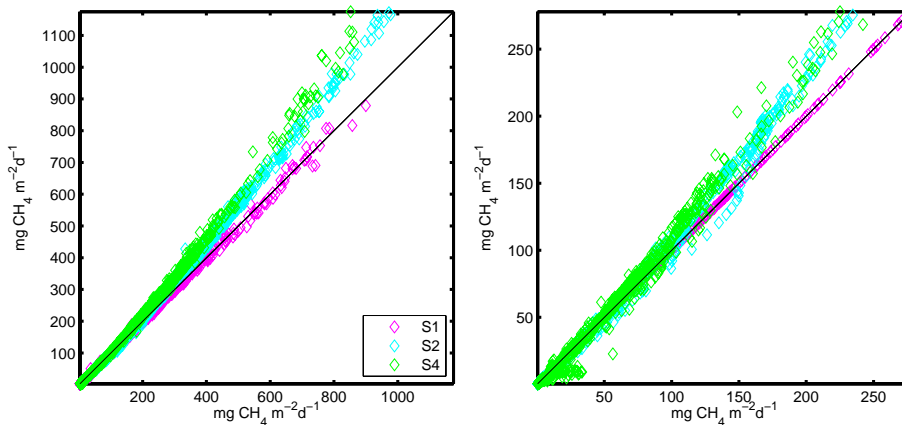
Fig. 11. Impact of temperature dependence of phase-related parameters on the CH_4 efflux simulations with models of different complexity at: **(a)** Buck Hollow site; **(b)** Big Cassandra site. The black line denotes where $y=x$. The results from standard simulations were plotted *abscissa*.

Fig. 12a. Methane effluxes, component-wise emissions and pore water concentration profiles from one-substance model (S1 model) in test simulations using a linear root distribution function. **(a)** Panels for the Buck Hollow site. **(b)** Panels for the Big Cassandra site. Dashed lines indicate the level of water tables.
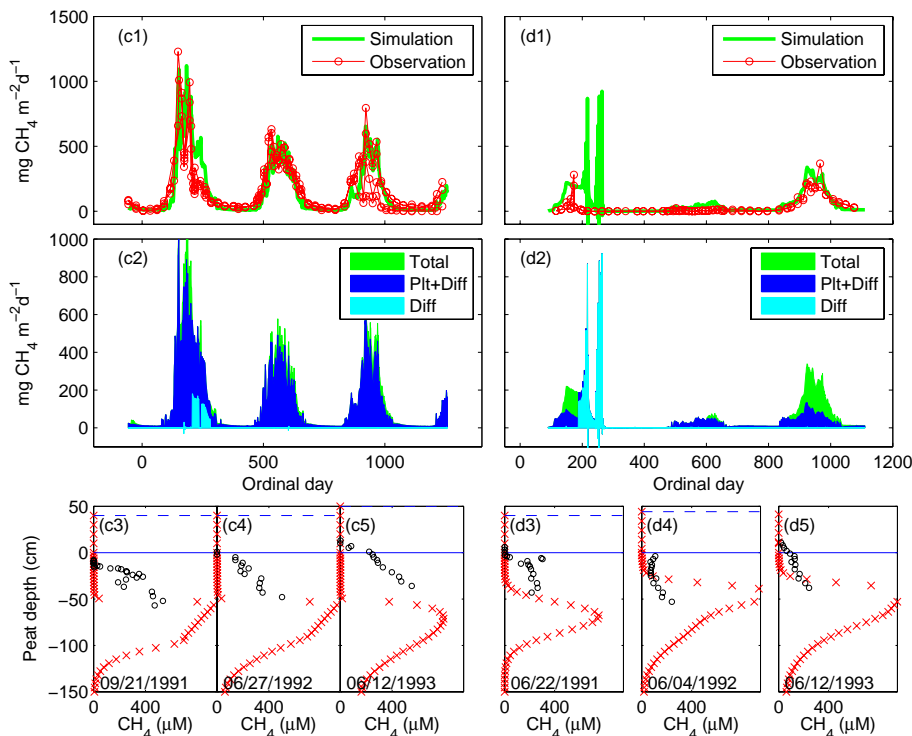
Fig. 12b. Methane effluxes, component-wise emissions and pore water concentration profiles from two-substance model (S2 model) in test simulations using a linear root distribution function. **(c)** Panels for the Buck Hollow site. **(d)** Panels for the Big Cassandra site. Dashed lines indicate the level of water tables.
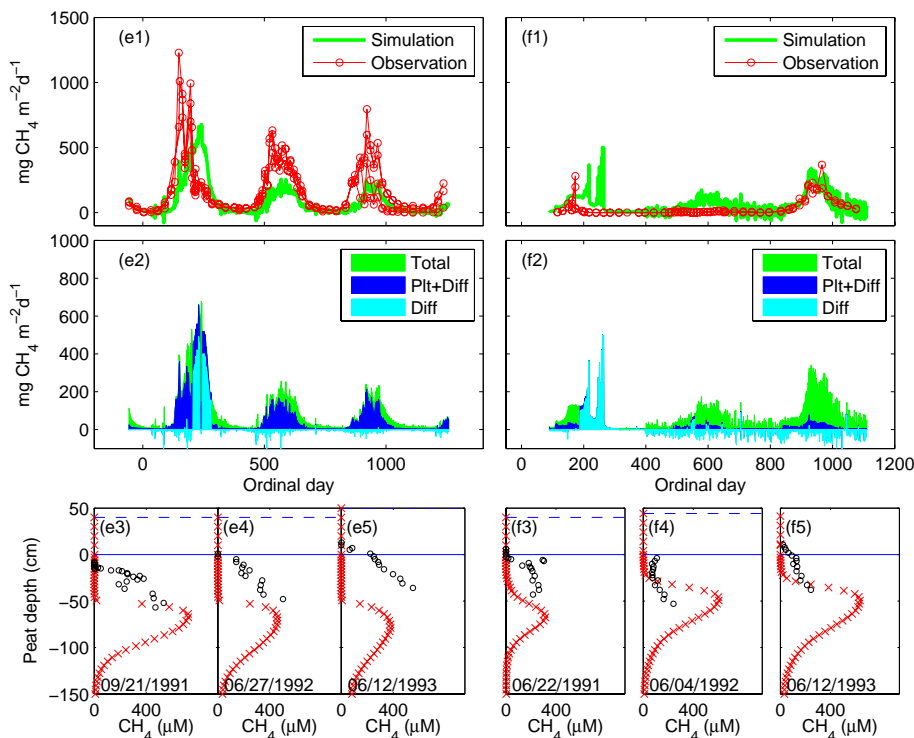
Fig. 12c. Methane effluxes, component-wise emissions and pore water concentration profiles from four-substance model (S4 model) in test simulations using a linear root distribution function. **(e)** Panels for the Buck Hollow site. **(f)** Panels for the Big Cassandra site. Dashed lines indicate the level of water tables.